12

Carbon Nanofibers Reinforced Ceramic Matrix Composites

Pavol Hvizdoš, Viktor Puchý, Annamária Duszová and Ján Dusza
Institute of Materials Research, Slovak Academy of Sciences, Slovakia

1. Introduction

Modern ceramic materials have, thanks to their crystallographic structure and strong atomic bonds, many excellent properties, such as extremely high hardness, strength, high thermal and chemical stability, high corrosion resistance, and wear resistance. Their weakness is low fracture toughness and crack growth resistance and hence high brittleness and lower reliability. One of the ways how to overcome these drawbacks is preparation of composite materials, where the base ceramic matrix is reinforced by secondary phases in forms of particles/whiskers and in recent years increasingly in a form of fibrous structures. In advanced fine grained ceramics these usually take form of nanofibers and/or nanotubes.

Among the most promising candidates are carbon-based filamentous nanomaterials such as carbon nanotubes (CNTs) and also carbon nanofibers (CNFs), which attracted a lot of attention due to their outstanding mechanical properties, excellent thermal performance and useful electrical characteristics (high electrical conductivity).

Nowadays, new ceramic/carbon nanotube composites are being developed mostly with two aims: to improve the mechanical properties of the ceramic materials by reinforcing with carbon nanofibers and to develop functionalized ceramics with improved magnetic and electric properties. Studies show that CNTs (both single-wall and multi-wall) should be ideal reinforcing/functionalizing elements for composites due to their small size, low density and good electrical and thermal conductivity.

This work focuses on investigations of ceramic matrix composites based on alumina, zirconia and silicon nitride reinforced by carbon nanofibers and nanotubes. The basic characteristics of commercially available nanofibers/nanotubes are studied by various techniques.

The chapter then focuses on mechanical properties of reference monolithic and experimental composite materials. The effect of volume fraction of carbon nanofibers on hardness and fracture toughness is illustrated. Further, the possibilities of improving the tribological and wear properties are discussed. The chapter concludes with the section that explores important aspect of functionalization of ceramics composites by improving their electrical properties, namely electrical conductivity.

2. Description of constituents

Recently a lot of experimental work and development has been going on in preparation of ceramic matrix composites with carbon nanofibers as great improvements of material

properties are expected. Up–to-now only modest enhancement of properties have been reported in CNT reinforced silicon carbides (Ma et al., 1998) and silicon nitride (Balázsi et al., 2003; Belmonte et al., 2010). Some other works reported improved fracture toughness achieved in alumina matrix systems (Zhan et al., 2003a) but rather often the performance of new composite materials was disappointing due to difficulties in dispersing the CNTs in ceramic microstructures and rather weak bond with them. More success has been achieved in increasing the electrical conductivity in many originally insulating ceramic materials (Zhan et al., 2003b, Balázsi et al., 2006) and in optimizing tribological behaviour of brittle systems (González-Julián et al., 2010; Hvizdoš et al., 2010).
This section describes basic characteristics of alumina, zirconia and silicon nitride as materials of ceramic matrices and provides the information about the ongoing effort in combining these materials with carbon nanofibers and nanotubes.

2.1 Aluminium oxide

Aluminium oxide (Al_2O_3), commonly referred to as alumina, is the most cost effective and widely used material in the family of engineering ceramics. The raw materials from which this high performance technical grade ceramic is made are readily available and reasonably priced, resulting in good value for the cost in fabricated alumina shapes. With an excellent combination of properties and an attractive price, it is no surprise that fine grain technical grade alumina has a very wide range of applications.
Alumina possesses strong ionic interatomic bonding giving rise to its desirable material characteristics. It can exist in several crystalline phases which all revert to the most stable hexagonal alpha phase at elevated temperatures. This is the phase of particular interest for structural applications. Alpha phase alumina is the strongest and stiffest of the oxide ceramics.
Among its key properties one can emphasize high hardness and wear resistance, excellent dielectric properties from DC to GHz frequencies, resistance to strong acid and alkali attack at elevated temperatures, good thermal conductivity, excellent size and shape capability, high strength and stiffness. The material is industrially available in purity ranges from 94% (an easily metallizable composition), to 99.5% for the most demanding high temperature applications.
Typical uses of alumina include gas laser tubes, wear pads, seal rings, high temperature electrical insulators, high voltage insulators, furnace liner tubes, thread and wire guides, electronic substrates, ballistic armor, abrasion resistant tube and elbow liners, thermometry sensors, laboratory instrument tubes and sample holders, instrumentation parts for thermal property test machines, grinding media, etc.

2.2 Zirconium oxide

For polycrystalline zirconia ceramics is typical combination of high strength, fracture toughness and chemical stability, which enables its use in extreme conditions (Garvie et al., 1975). It is an extremely refractory material which can be used at temperatures up to 2400°C. It offers chemical and corrosion inertness to temperatures well above the melting point of alumina. It has relatively high density and low thermal conductivity (20% that of alumina). It resists molten metals and has high wear resistance. It is electrically conductive above 600°C and is used in oxygen sensor cells and as the susceptor (heater) in high temperature induction furnaces, where it can be used at over 2000°C in oxidizing atmospheres. Other typical uses include cutting tools for cutting problematic materials such as Kevlar, polymer

films and paper. It is an attractive material for nuclear industry, where it is used for inert matrices for plutonium storage and as immobilizer of nuclear waste. Another applications include seals and pistons in pumps for chemically aggressive and abrasive suspensions, bearings, biomedical implants, e.g. dental, hip, and knee joints (Garvie et al., 1984), and thermal barriers coatings (using plasma sprayed TBCs the working temperature of thermally exposed parts, such as gas turbine blades, can be increased of about 200°C).

2.3 Silicon nitride

Silicon nitride (Si_3N_4) is a man made compound synthesized through several different chemical reaction methods. Parts are pressed and sintered by well developed methods to produce a ceramic with a unique set of outstanding properties. Silicon nitride has relatively high strength and fracture toughness, low density (3.2 $g.cm^{-3}$), good corrosion and oxidation resistance at room and elevated temperatures thanks to presence of surface layer of SiO_2. It has quite good thermal shock resistance thanks to low thermal expansion coefficient (3.1 ÷ 3.6 x 10^{-6} K^{-1} from room temperature up to 1000°C).

Silicon nitride can not be sintered directly, because above 1850°C at 0.1 MPa it dissociates. One of the common methods of preparation Si_3N_4 bulk ceramics is reaction sintering, its product is called reaction-bonded silicon nitride (RBSN).This methods is based on heating of silicate powder compact in nitrogen atmosphere. The resulting material tends to have higher open porosity. Hot pressing and hot isostatic pressing sinter the silicon nitride powders at temperatures 1700 to 1800 °C with oxides, which form liquid phase, as sintering additives and produce fully dense materials. Microstructure of resulting materials consists of fine grains of α-Si_3N_4 and larger β-Si_3N_4 with higher aspect ratio. Such microstructures are desired for high strength and better fracture toughness (Morrell, 1985).

Silicon nitride is a rather expensive material, but its performance to cost benefit ratio is excellent in the applications where it can outperform the normally utilized materials with long life and very reliable low maintenance operation. It has outstanding wear resistance in both impingement and friction modes.

High performance silicon nitride materials were developed for automotive engine wear parts, such as valves and cam followers and proven effective. The cost of the ceramic parts never dropped enough to make the ceramics feasible in engines and turbochargers. The very high quality bodies developed for these demanding high reliability applications are available today and can be used in many severe mechanical, thermal and wear applications.

2.4 Carbon nanotubes (CNT) and carbon nanofibers (CNF)

Carbon nanofibers CNFs are cylindrical or conical structures that have diameters varying from a few to hundreds of nanometers and lengths ranging from less than a micron to millimeters. The internal structure of carbon nanofibers varies and is comprised of different arrangements of modified graphene sheets. A graphene layer can be defined as a hexagonal network of covalently bonded carbon atoms or a single two-dimensional 2D layer of a three-dimensional 3D graphite Fig. 1a. In general, a nanofiber consists of stacked curved graphite layers that form cones Fig. 1b or "cups." (Krishnan et al., 1997; Endo et al., 2002) The stacked cone structure is often referred to as herringbone or fishbone while the stacked cups structure is most often referred to as a bamboo type, resembling the compartmentalized structure of a bamboo stem. Currently there is no strict classification of nanofiber structures. The main distinguishing characteristic of nanofibers from nanotubes is the stacking of graphene sheets of varying shapes.

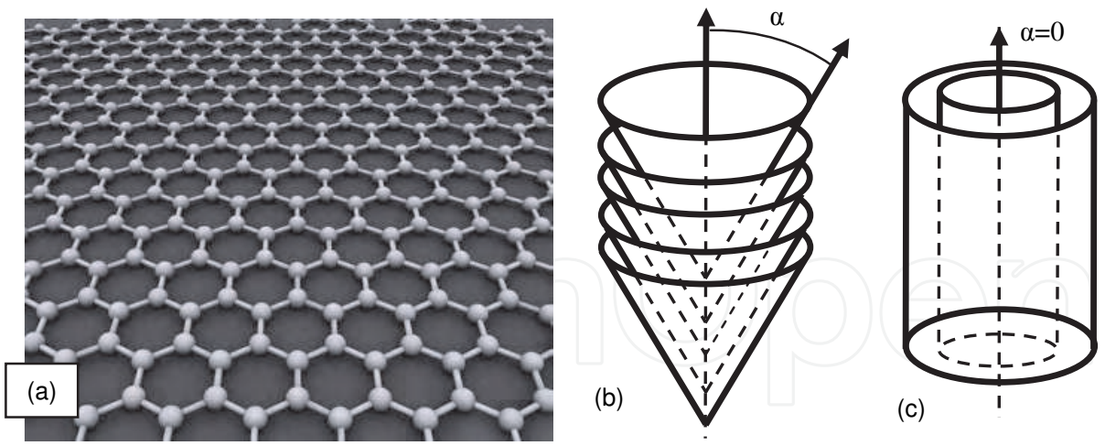

Fig. 1. Schematic structure of carbon nanofibers and nanotubes. (a) Graphene layer, (b) stacked cone (herringbone) nanofiber, and (c) nanotube. After (Melechko et al., 2005).

We can define α as an angle between the fiber axis and the graphene sheet near the sidewall surface Fig. 1b. The nanofiber with α=0 is a special case in which one or more graphene layers form cylinders that run the full length of the nanostructure, Fig. 1c. This arrangement, with its closed and semi-infinite surface, discovered and endorsed by Iijima (Iijima, 1991), results in extraordinary properties that made this type of a nanofiber known to the world as a carbon nanotube CNT.

The chemical properties of nanofibers and nanotubes are quite different since defect-free nanotube walls do not contain the exposed edges and unsaturated bonds of graphene planes (compare Fig.1 b and c), and as a result nanotubes are far less reactive than nanofibers. The scientific community and the popular press have focused more on the special case of the CNT structure than the more general case that includes nanofibers. The reason for the attention given to nanotubes is clear: the beauty and perfection of their mathematical description and the resulting extraordinary mechanical and electron-transport properties.

2.4.1 Mechanical properties of CNTs and CNFs

Important characteristic of most materials is that a small diameter (nanoscale) fiber is much stronger than the bulk material, (Callister, 2003) due to the lower probability of critical surface flaws with decreasing specimen volume. The majority of engineering forms of carbon have more or less disordered graphite microstructures. The microstructure of the crystalline layers within the fiber influences properties such as strength, stiffness, deformation modes, fracture behavior, and toughness, (McEnaney, 2001). The literature shows great variance in the mechanical properties of carbon forms such as carbon nanotubes and carbon fibers. (Melechko et al., 2005) gives some general ranges for the strength and modulus of engineering carbons. The high volumetric density of short, strong sp3 bonds gives diamond the highest stiffness of any known materials (Young's modulus ~ 1 TPa). Single crystal graphite has a Young's modulus over 28 times higher in the direction parallel to the basal planes than in the perpendicular direction. Thus, while there is a preferred orientation of basal planes parallel to the fiber axis, this creates poor transverse properties. Carbon fibers can also have as high as 100 times more stiffness along the fiber axis than perpendicular to it, (McEnaney, 2001). Single-crystal carbon nanotubes have extremely large length-to-diameter aspect ratios, with diameters as small as only a few nanometers. They are

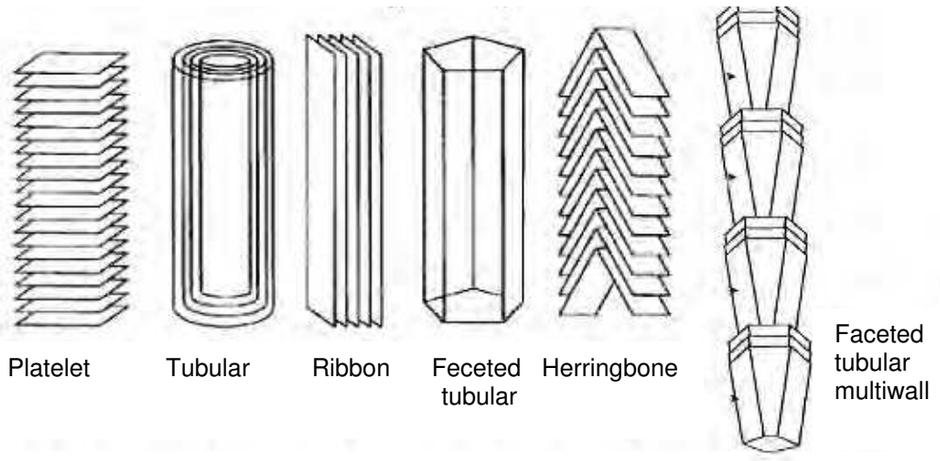

Fig. 2. Typical structures of CNFs, after (Al-Saleh, 2009).

the strongest known material, with a specific tensile strength as high as 100 times that of steel, (Ruoff et al., 2003). For SWCNTs, tensile strengths range between 50 and 200 GPa, Young's modulus is on the order of 1 TPa and fracture strains are between 5% and 20%. As a consequence of their size and high degree of crystalline perfection, CNTs are virtually flaw-free, which contributes to their exceptional strength. However, in spite of their incredible mechanical properties, SWCNTs are not utilized extensively as a reinforcement medium because they are expensive to produce and purify. On the other hand, MWCNTs are easier to produce since they do not require as stringent catalyst particle preparation. MWCNTs are composed of concentric graphene sheets and have diameters on the order of tens of nanometers depending on the number of graphite layers. One drawback is that these layers can slide past each other easily, often failing by the "telescoping" mechanism, (Yu et al., 2000). This failure and the increased probability of defects with greater mass make MWCNTs less desirable than SWCNTs, but their strength still surpasses that of steel and they have a high modulus.

Carbon fibers, composed of polycrystalline and amorphous carbon, have diameters ranging from hundreds to thousands of nanometers and can be grown thousands of micrometers long. Crystallographically, they can be found in many forms (Fig. 2). Their tensile strengths are about an order of magnitude lower than for CNTs, ranging from 1.5 to 4.8 GPa and the Young's modulus is between 228 and 724 GPa, (Callister, 2003). Carbon fibers retain their high tensile modulus and strength at elevated temperatures and are not affected by water, solvents, acids, or bases at room temperature. Even though their mechanical properties are not as astounding as those of carbon nanotubes, carbon fibers are relatively easy to produce as well as economical.

2.5 Preparation of ceramic matrix composites with carbon nanofibers

The processing steps of advanced ceramics include powder synthesis, preparation of the powders mixture (mixing, milling, etc.), forming (pressing, injection moulding, slip casting, etc.) and sintering (pressureless sintering, hot pressing, hot isostatic pressing, etc.). In the following we will summarize the processing steps used for the preparation of ceramic-CNTs/CNFs composites.

The inclusion of CNTs in a ceramic matrix is expected to create composites exhibiting high toughness and improved mechanical properties compared to the single-phase ceramic

material (Mukhopadhyay et al., 2010). Ideally, the CNTs dispersed in a ceramic matrix should serve as sites for fracture energy dissipation through mechanisms such as crack deflection and nanotube debonding/breakages, (Dusza & Šajgalík, 2009). Hot-pressing of ceramic powder mixed with CNT is the most common method to prepare such composites.
Hot-pressing is mostly applied in the pressure range of 20–40 MPa and at temperatures of 1300–2000 ^{o}C, but slip casting and injection molding followed by pressureless sintering is also used. There are only a limited number of authors dealing with the hot-pressing processing of CNT/ ZrO_2 composites.
Spark plasma sintering is a new process where ceramic powder can be sintered very fast to full density. It is similar to hot-pressing which is carried out in a graphite die, but the heating is accomplished by spark discharges in void between particles generated by an instantaneous pulsed direct current applied through electrodes at the top and bottom punches of the graphite die. Due to these discharges, the particle surface is activated and purified, and a self-heat phenomenon is generated between the particles, thus the heat-transfer and mass-transfer can be completed instantaneously, (Perera et al., 1998). SPS use heating and sintering temperature at 1000-1800 ^{o}C, at a heating rate of 500-600 ^{o}C/min under a pressure of 40-60 MPa and than fast cooling to 600 ^{o}C/2-3min.

2.5.1 Processing of ZrO_2-based ceramic-CNT composites

Fully-dense 3 mol. % yttria stabilized tetragonal polycrystalline zirconia (3Y-TZP) matrix composites containing 0.1–1 wt. % of MWCNTs and SWCNTs were fabricated by SPS at 1300 °C for 5 min, under an applied pressure of 20 MPa, (Sun et al., 2005).
MWCNT/3Y-TZP composites with different MWCNT contents were prepared by SPS by several groups (Shi & Liang, 2006; Mazaheri et al., 2011). The DC conductivity of the composites was found to follow a typical percolation behavior with a very low percolation threshold between 1.0 and 2.0 wt. % MWCNT content. The dielectric constant was greatly increased when the MWCNT concentration was close to the percolation threshold, which was attributed to dielectric relaxation, the space charge polarization effect, and the percolation effect. The electrical conductivity of a composite prepared by dispersing multiwall carbon nanotubes in yttria-stabilized tetragonal zirconia matrix, and subsequent spark plasma sintering, was investigated by Shi and Liang in 2007 (Shi & Liang, 2007). The experimental analysis of the effect of temperature on the conductivity suggested that for temperatures higher than 35 K, conduction can be attributed to thermal fluctuation-induced tunneling of the charge carriers through the insulating zirconia separating by the multiwall carbon nanotube clusters.
Sun et al., 2005, reported the CNTs-3Y-TZP composite powder sintered by SPS. The prepared composite powder was carefully placed into a 20 mm diameter graphite die, and heated to the sintering temperatures at 1300 °C for 5 min. A pressure of approximately 20 MPa was applied from the beginning of sintering and relaxed after the temperature below 800 °C. The composites with the content of carbon nanotubes ranging from 0.1 to 1 wt. % were prepared. It was found that the hardness values decreased prominently with the addition of CNTs. The fracture toughness kept almost the same value as that of the matrix when the amount of MWCNTs was kept 0.5 wt. %, however it decreased to 4.47 MPa $m^{1/2}$ when the MWCNTs content was raised to 1.0 wt. %. 0.5 wt. % SWCNTs-3Y-TZP composites showed no improvement on the mechanical properties of 3Y-TZP either. The existence of the agglomerated CNTs in the grain boundary and the weak bonding between carbon nanotube and zirconia matrix were reasons that led to the failure in reinforcement.

An alternative route for the synthesis of ceramic–CNT composites is a process, where the CNTs act as nucleation sites for the ceramic. Lupo et al., 2004, reported the successful application of such a route to prepare ZrO_2, which is grown on carbon nanotubes by a hydrothermal process. The hydrothermal process employs high temperatures and high pressures for the crystallization of hydroxide into the oxide [$Zr(OH)_4 \rightarrow ZrO_2+H_2O$]. The end product consisted of CNTs coated with nano-sized ZrO_2 particles. Other interesting approaches include the process involving direct in-situ growth of MWNTs on zirconia particles (Datye et al., 2010) or colloidal processing (Garmendia et al., 2010).

2.5.2 Processing of Al_2O_3-based ceramic-CNT composites

Alumina based materials are usually prepared by conventional methods, as they are generally easy to sinter. When using the pure carbon phases, special care is necessary, so that they are not destroyed in the process. Inam (Inam et al., 2010) developed alumina–carbon black and alumina–CNTs composites with the aim to improve the electrical conductivity of the alumina. Multi-wall CNTs with average outer diameter 9.5 nm; lengths of up to 1.5 μm; and density 1.7 $g.cm^{-3}$) were dispersed in dimethylformadie, DMF using high power sonication for 2 h and then hand-mixed with alumina nanopowder with particle size <50 nm; surface area 35–43 $m^2.g^{-1}$; melting point 2040 °C; and density 3.97 $g.cm^{-3}$) for 2 min. Since DMF was found to be a much more effective dispersant than ethanol for making stable, homogeneous CNT and composite dispersions. The liquid mixture was rotation ball milled for 8 h. It was then dried at 75 °C for 12 h on a heating plate in air, followed by in a vacuum oven at 100 °C for 3 days. The dried agglomerated mixture was ground and sieved and then placed again in the vacuum oven at 100 °C for another 4 days to thoroughly extract the solvent. Alumina and nanocomposite pellets were prepared by SPS in a HPD 25/1 furnace. A pressure of 100 MPa was applied concurrently with the heating (rate 300 °C/min) and released at the end of the sintering period, which was 3 min for all of the samples.

Cha et al., 2005, used MWNTs, fabricated by chemical vapor deposition for the preparation of the composites. The CNTs were acid-treated, oxidized at 190 °C for 4 h to remove catalysis particles and to generate functional groups on the surfaces of the nanotubes. The acid-treated CNTs were sonicated in distilled water for homogeneous dispersion. $Al(NO_3)_3 \bullet 9H_2O$ was added into a suspension with the CNTs and these were sonicated. This solution was vaporized and the powders that remained were oxidized in air atmosphere. The volume fractions of CNTs varied from 0 to 1.8 vol. %. During the calcination process, the chemical bonding between CNTs and the amorphous Al_2O_3 matrix was formed. SPS was used for densification. The composite powders were compacted in a graphite mold with a diameter of 8 mm and were heated by pulsed electric current at a vacuum pressure of 1 Pa. The heating rate was fixed for 100 °C/min. Alumina–CNT composite powders were synthesized in the catalytic decomposition of acetylene over alumina powders impregnated with iron catalysts by An et al., 2003. The alumina, MgO, and $Fe(NO_3)_3 \bullet 9H_2O$ powder were mixed by planetary ball milling to prepare the alumina powder impregnated with iron catalysts. The powder was mixed in ethanol by alumina balls. After ball milling, the ethanol solution was removed via rotary evaporation. The materials were then heated overnight followed by grinding into a fine powder. For the CNT synthesis, each alumina powder having four different iron catalyst contents were placed in an alumina boat mounted in a tube furnace.

Lim et al., 2005, used CNTs produced by the catalytic decomposition. The ceramic powders were mixed by planetary ball milling in ethanol then hot pressed for 1 h at 2123 K under 30

MPa. For some samples a modified tape casting method was employed for dispersing the CNTs. Tape casting slurry was prepared by using a planetary ball milling. Metylisobutyl-ketone, KD-1, polyvinyl-butyral, and di-butyl phathalate were used as solvent, dispersant, binder, and plasticizer, respectively. After the binder burnout, the sample was hot pressed at 2123 K under 30 MPa for 1 h.

2.5.3 Processing of Si_3N_4-based ceramic-CNT composites

Tatami et al., 2005, used highly pure and fine Si_3N_4 powder as a raw material together with Y_2O_3 AlN and TiO_2 as sintering aids. MWNTs were added as an electrical conductor. The amount of CNTs was changed from 0 to 12 wt. % of the total amount of the other raw powders. Three wt. % of dispersant was added to ethanol, whose ratio was 63.3 mg to 1 g of CNT to prepare a slurry using an ultrasonic vibrator. The slurry was mixed with the Si_3N_4–Y_2O_3–Al_2O_3–AlN–TiO_2 slurry with 2 wt. % of the dispersant and then prepared by ball milling. After mixing, the ethanol in the slurry was evaporated and the mixed powder was sieved to obtain granules. The granules were molded followed by cold isostatic pressing at 200 MPa. After dewaxing, the green bodies were gas pressure sintered (GPS) at 1800 °C for 2 h in 0.9 MPa N_2. For more densification, HIP was used at 1700 °C for 1 h under 100 MPa.

In the study of Balázsi (Balázsi et al., 2004) the compositions of the starting powder mixtures of the investigated materials were: 90 wt. % Si_3N_4, 4 wt. % Al_2O_3, and 6 wt. % Y_2O_3. In addition to batches of MWNTs, carbon black, graphite, and carbon fibers were added. The powder mixtures were milled in ethanol in a planetary type alumina ball mill for several hours. Each batch contained approximately 1 g alumina as contamination from balls and jars. After milling, the powder mixtures and CNTs were introduced in an ethanol bath and sonicated together. Samples were compacted by dry pressing at 220 MPa. The materials were sintered at 1700 °C in high purity nitrogen by a two-step sinter-HIP method using BN embedding powder.

3. Testing methods

3.1 Nanotubes and nanofibers characterization

The morphology and structure of nantubes and nanofibers were characterized by scanning and transmission electron microscopy. For examination of length, diameter and outer morphology usually field emission SEM was used. TEM and HR-TEM was employed to observe the crystal structure and graphene layers arrangement. The TEM specimens have been prepared by dispersing the CNFs in an acetone ultrasonic bath and dropping a suspension onto a carbon lace Cu grid. The TEM images and selected area electron diffraction patterns were recorded using an accelerating voltage of 200 kV.

3.2 Ceramic composites characterization

Microstructure studies of bulk composite materials were carried out also using high resolution SEM, TEM and HR-TEM. The SEM studies were done on samples that were prepared by diamond cutting, polishing and usually thermal etching in order to reveal the grain structure, topography and distribution of individual phases. Sometimes also fracture surfaces were observed as they can convey the information about 3D characteristics of the microstructure as well as about the cohesive and bonding characteristics of matrix grains and CNFs which determine the type of fracture and crack propagation.

X-ray diffraction (XRD) analysis was used for the determination of phase composition of final experimental composite materials.
Mechanical characterization was done in terms of measurement of basic mechanical properties of bulk composite materials such as hardness and fracture toughness by indentation method. Hardness is a measure of the material resistance against deformation by a hard body (indenter) driven into its surface. In ceramic materials it is measured most often by Vickers method where the indenter is a defined four-sided diamond pyramid. Vickers hardness (HV) is calculated according to the standard formula

$$HV = 1.8544\ F / d^2 \quad (1)$$

where F denotes the indentation load, d is the length of the indentation impact diagonal.
Fracture toughness (K_{IC}) expresses the resistance of the material against sharp crack propagation. In brittle materials it is possible to determine it from the length of the cracks emanating from the corners of the indents produced by sharp indenters (e.g. Vickers). This method has the advantage that it can be used to probe very small specimens of irregular shapes. This is often the case for new materials which are just being developed and the specimens required for other standardized and better defined methods are unavailable. The disadvantage of this type of tests is that the stress states creating the cracks are very complicated and difficult to describe analytically. There exist many phenomenological formulas relating fracture toughness to indentation crack lengths. For very brittle materials such as zirconia and alumina based ceramics, and also for very fine grained silicon nitride composites, the cracks were shown to have usually half-elliptical shape. In this case one of the most suitable is a formula proposed by (Anstis et al., 1981):

$$K_{IC} = \eta\ F\ (E/H)^{1/2} / c^{3/2} \quad (2)$$

where η is a geometric factor, E is the modulus of elasticity, H is the hardness expressed as pressure (i.e. in Pa), and c is the indentation radial crack half-length at the surface.
Wear behaviour of the experimental materials was studied in most cases in sliding against specific tribological partner or for self-mated pairs. In this sort of tests the surfaces were carefully prepared by polishing down to surface roughness below 1 μm. The tangential forces are measured during the test and friction coefficients are calculated. The worn surfaces are subsequently observed and the wear regimes, damage type and micromechanisms are identified. If possible the material losses due to wear are measured and then specific wear rates (W) can be calculated according to the standard (ISO 20808, 2004) as the volume loss (V) per distance (L) and applied load (F_p):

$$W = V / (L\ F_p) \quad (3)$$

The electrical conductivity measurements were carried out at ambient temperature using a two-point probe setup on an impedance analyzer at frequencies from 40 Hz to 40 kHz.

4. Properties

4.1 Microstructure

As mentioned before, carbon nanofibers can have many various crystallographic structures. A series of studies (Duszová et al., 2008a; Dusza et al., 2009; Puchý et al., 2010) was done on commercial grades of CNFs made by catalytic chemical vapour deposition (CCVD), which

produces a good variety of high quality materials. The morphology of these types of carbon nanofibers is illustrated in the Figs. 3 and 4. The SEM images reveal that the CNFs are typically rope – like shaped with tubular structure and with the outer diameter of 50 – 250 nm and inner diameter from 20 nm to 230 nm. According to the SEM observation the length of the CNFs is up to several μm and the fibers are separated with the characteristic rope-shape. In several cases we found clusters of the fibers with crooked and entangled fibers, too. The majority of the fibers have a diameter from 200 to 300 nm. Beside the elongated carbon nanofibers (Fig. 3a) occasionally particle shaped carbon objects with the maximal size of several micron have been identified. Two basic types of nanofibers have been identified by SEM observation; conical hollow rope – type tubes, usually with a free ends and smooth surface and bamboo shaped nanofibers with waved surface, Fig. 3b. The third type of nanofibers with a straight line shape and rough surface was identified only randomly. Observation of the end of the rope - fibers revealed that the diameter of the hole in the fiber is different and the wall of the fibers consists from layers with different structure.

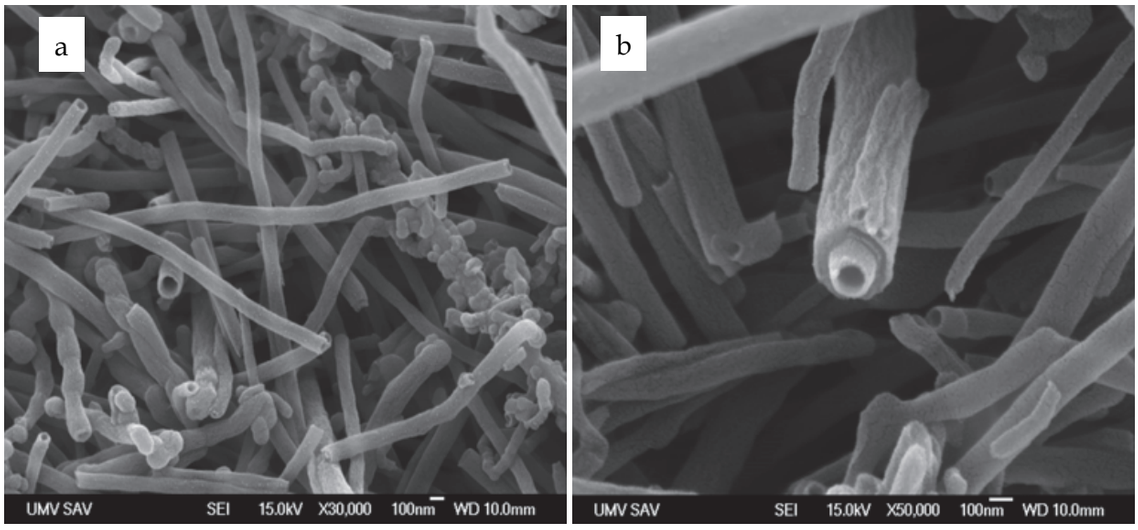

Fig. 3. Morphology of the carbon nanofibers, mix of rope-like and bamboo shaped nanofibers (a), example for smooth small and rough large diameter nanofibers (b), SEM, (Puchý et al., 2010).

The study of the surface morphology of the fibers revealed that the fibers with smaller diameters are smoother comparing to the fibers with larger diameters. Lee et al., 2007, investigated the surface morphology of hollow and solid as received, heat – treated and CVD surface treated fibers and found that the solid fibers exhibited rougher surface comparing to the hollow fibers in all forms. Measurement and statistical evaluation of the distribution of the diameters of nanofibers show that their diameter varied from 50 to 600 nm with the average diameter equal to 120 nm.

Results of TEM are in a good agreement of the results of SEM and it can be seen that in the case of straight pipe-shaped fibers the wall is smooth and uniform and consists from distinct sandwich of graphite layers. In this case the graphene layers are parallel to the axes of the fibers and form usually defect free material. The bamboo-shaped fibers are composed of

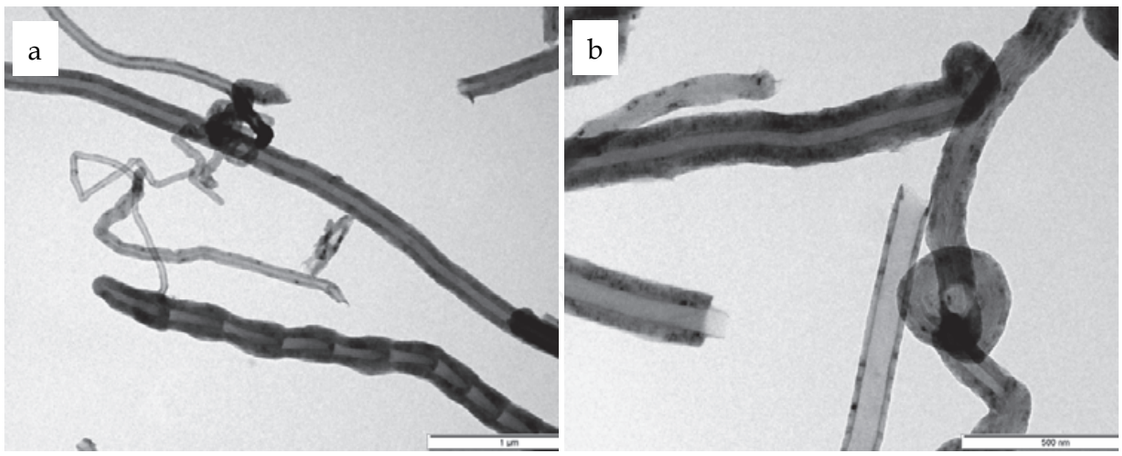

Fig. 4. Characteristic morphology of CNFs by TEM, rope like and bamboo – like CNFs (a), CNT with the root and broken CNT with longer inner layer (b), (Puchý et al., 2010).

multi – walled graphite structure and the bamboo sections have a size parallel with the axes of the fibers 2-3 times larger comparing to the outer diameter of the fibers. It seems that the carbon diffusion was not continuous at the all fibers during they growth, leading to a pulsed growth which translated into a periodic variation of the fibers diameter as it is illustrated in Fig. 4. Such bamboo–shaped fibers are composed of hollow segments of a size approximately 100 nm deliminated by curved stacking of carbon sheets. Longtin et al., 2007, prepared bamboo-type nanofibers by laser-assisted catalytic vapor deposition applying two different catalyst preparation methods and the nanofibers analyzed using SEM, HREM and Raman spectroscopy. Using approximately 50 nm thick deposited catalyst layer within the pores of an alumina substrate results in an array of vertically aligned nanofibers with similar dimension as the analyzed nanofibers in the present work. The lattice fringe analysis of HREM indicated that pulsed growth at high rates leads to bamboo-type nanofibers having oriented graphitic domains similarly as in our case. Bamboo-shaped carbon-nitrogen nanotubes have been prepared by Lee et al., 2002, using pyrolysis of iron pentacarbonyl and acetylene mixture with ammonia and by pyrolisis of melamine with NaN_3-Fe-Ni. They showed that the nitrogen doping leads to the origin of the bamboo-like structure and results in the degraded crystallinity of graphite sheets. By TEM they found that in the bamboo-like CN nanofibers the wall thickness increases due to the generation of compartment layers, but the outer diameter remains constant. This is different comparing to the bamboo-like carbon nanofibers characterized in the present investigation when the outer diameter of the nanofibers increased during the generation of compartment layers due to the changed orientation of the graphite sheets.

The internal structure of the fibers is related to the orientation of the graphite sheets as illustrated in Figs 5, 6 (Puchý et al., 2010). The fiber illustrated in Fig. 5 has a wall thickness of 28 nm and hole diameter of 30 nm.

HREM shows that the graphene structure of the wall parallel to the axes in some cases is similar to the pipe–shaped fibers but sometimes these fibers consists of a wall from areas with differently oriented graphite layers. Many different orientations (Fig. 6) of such layers were identified, from parallel up to very high inclinations (Lee et al., 2007; Duszová et al., 2008a, etc.). Besides, some edge graphite planes can be formed in single or multi loops whereas some end planes are strongly undulated.

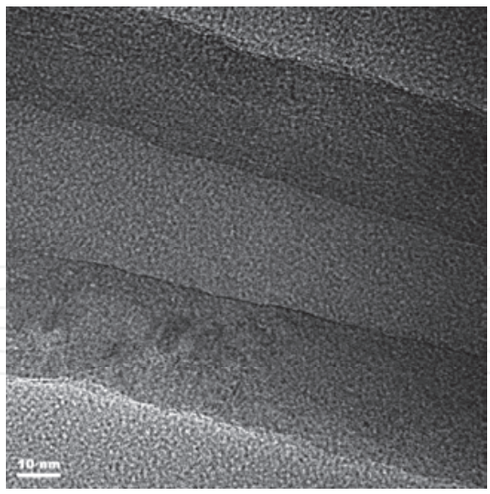

Fig. 5. HREM of a pipe – shaped conical hollow nanofiber with the wall thickness approximately 28 nm and hole diameter approx. 30 nm. The interlayer spacing of the graphite layers is approx. 0.35 nm.

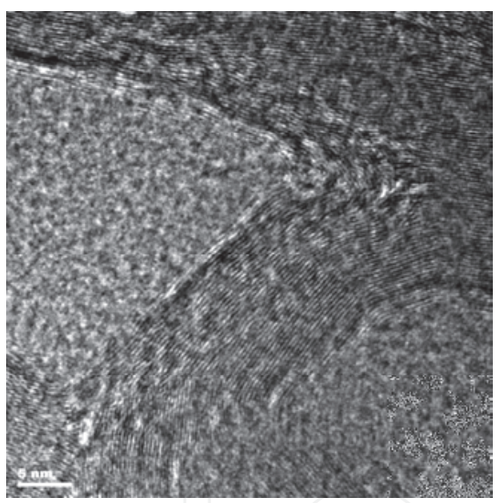

Fig. 6. HREM of a bamboo – shaped nanofiber with the wall thickness approximately 18 nm. The interlayer spacing of the graphite layers in this wall is approximately 0.33 nm (Puchý et al., 2010).

Hot pressed ZrO_2-CNFs composite were systematically studied in (Duszová et al., 2008a; Dusza et al., 2009) where the authors compared their microstructure to a monolithic zirconia prepared in the same way. The hot-pressed monolithic zirconia exhibits nearly full density but the density of the ZrO_2–CNF composite was lower due to the porosity in the composite connected mainly with the clusters of the carbon nanotubes present in its microstructure. XRD analysis revealed that the experimental materials consist of mainly tetragonal ZrO_2, however a small amount of monoclinic zirconia and yttrium oxide has been found, too.

In Fig. 7 the microstructure of the monolithic hot-pressed zirconia and the composite is illustrated at lower magnification. The monolithic sintered and hot-pressed zirconia consists of very small, submicron/nanometer-sized grains with randomly occurring defects in the form of very small-sized pores with dimensions of approximately 100–200 nm, mainly in the

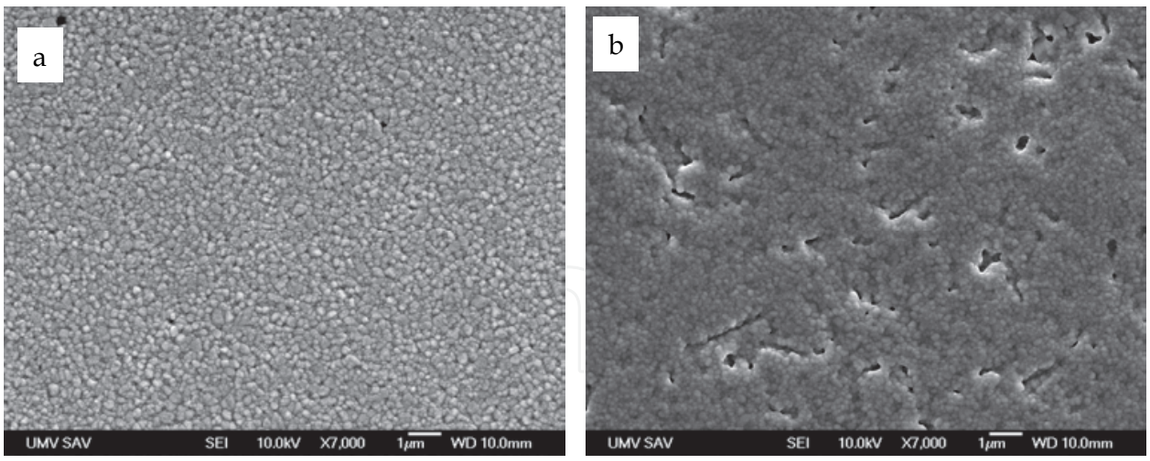

Fig. 7. SEM micrographs of the zirconia based experimental materials: microstructure of the HP monolithic zirconia (a) and HP ZrO_2 - CNFs composite at low magnification, thermally etched with the locations of the burned out CNFs during the thermal etching (b). (Dusza et al., 2009).

sintered material. The average grain size of the ZrO_2 in the sintered and hot-pressed zirconia is 190 nm and 162 nm, respectively. The microstructure of the composite consists of slightly smaller grained matrix with relatively well dispersed CNTs in the matrix, Fig. 7b (pores with their shape/orientation indicating the locations of the burned out CNTs during the thermal etching). The lower grain size of the zirconia together with the lower density of the composite compared to the monolithic material are evidence that the CNTs may hinder the sintering behavior of the zirconia-based composite.

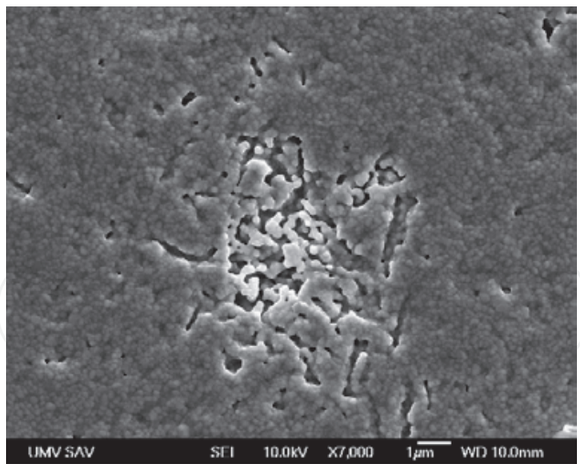

Fig. 8. Cluster of CNTs in the zirconia based composite, (Dusza et al., 2009).

Relatively high amount of clusters of the CNTs have been found on the polished surface and fracture surface of the samples indicating that the mixing procedure has to be improved. The size of the clusters varies from a few microns up to approximately 20 μm and porosity was always connected with these clusters (Fig. 8).

Balázsi with co-workers (Balázsi et al., 2006) developed CNT containing Si_3N_4 composites using hot isostatic pressing and compared them with the monolithic silicon nitride as well as

with composites containing carbon black and graphite prepared by identical procedure. They produced a series of composites with 1, 3, and 5 wt% of MWCNTs. All materials were carefully mixed, pressed at room temperature at 200 MPa and subsequently HIPed at 1700°C for various holding period (0 and 3 hrs) at 2 MPa or 20 MPa, respectively. They found that CNTs were preserved in the final structures. Problems with degradation of CNT, observed in other instances (Balázsi et al., 2003; Balázsi et al., 2004) were not observed in this newer work. The CNTs were located mainly in the inter-granular places and they were well attached to the silicon nitride grains as well as to each other. The proper separation and dispersion of carbon nanotubes proved to be a difficult task of composite preparation. The ball milling was followed by ultrasonic agitation of MWNT-powder mixtures for gaining a better homogeneity. By increasing the sonication time little advances have been achieved, but the tendency of nanotubes, the strong adherence and linking behavior to each other could not be totally suppressed. The CNTs in most cases remained in groups as nano- or micrometer sized islands in the matrix after sintering. By increasing the pressure from 2 to 20 MPa and holding time to 3 h a different microstructure could be developed. A grain growing process accompanied by a phase transformation was observed in 1 and 3 wt% CNT containing samples and large β-Si_3N_4 grains (several micrometers in length) formed. Generally, the CNT added samples had larger porosity than reference samples.

As regards the alumina based CMCs, this study focuses mostly on alumina-CNT composites prepared by SPS (Inam et al., 2010). For comparison also a monolithic Al_2O_3 ceramics was prepared by exactly same route.

The microstructure of the monolithic Al_2O_3 consists of relatively large, micron sized grains with randomly distributed submicrometric sized pores, located at the grain boundaries, Fig. 9a. Relatively large numbers of CNF clusters were observed on the polished and fracture surfaces of the Al_2O_3-3.5 % CNT composites, Fig. 9b. This material has much finer matrix with relatively well distributed carbon nanotubes with diameter of several nanometers and with very high aspect ratio. The smaller matrix grain size in the composite suggests that the carbon black and the CNTs hinder the grain growth during the sintering.

The CNTs in the Al_2O_3-CNT composite were located mainly in the intergranular places and were well attached to the alumina grains.

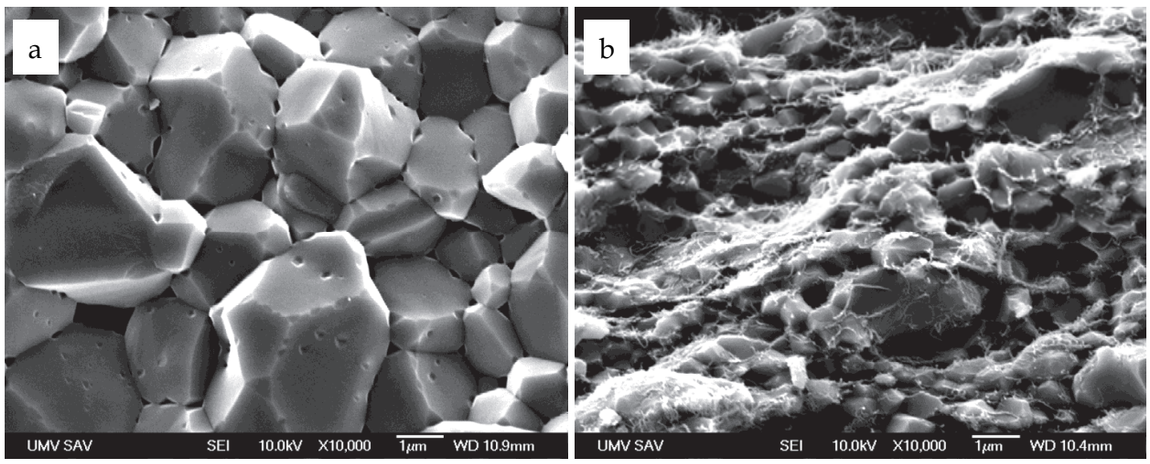

Fig. 9. Fracture surfaces of monolithic Al_2O_3 sintered at 1800 °C for 3 min under a pressure of 100 MPa (a) and alumina–3.5 wt.% CNT nanocomposite sintered at 1800 °C for 3 min under a pressure of 100 MPa (b).

4.2 Mechanical properties

As mentioned in the previous section, the CNT/Si_3N_4 prepared by Balázsi (Balázsi et al., 2006) had lower density (higher porosity) than the analogous reference sample. Consequently, the reinforcement processes (e.g. pullouts, crack bridging, crack deflection) were still not enough for a significant global strengthening. This resulted in decreasing values of modulus of elasticity and bending strength with increasing volume fraction of CNTs. By increasing the gas pressure (and holding time) the same level of densification can be achieved for composites with 1% CNT as for reference sample realised at low pressures (2 MPa). The modulus decreased from the value for silicon nitride (~250 GPa) linearly together with the apparent density regardless of the gas pressure used and for Si_3N_4-5%CNT with density around 2.2 $g.cm^{-3}$ it reached values between 50 and 100 GPa.

The relationship between apparent density and three point bending strength of composites has similar trend to the modulus namely, the decrease of strength with increasing the CNT content. In this case however, the effect of pressure and holding time was more pronounced and the materials prepared using higher sintering pressure (and holding time) were stronger. In the case of samples with 1% CNT content, applying a higher sintering pressure a higher compaction level and an increase by 100%, from an average strength level of 300–600 MPa, was achieved. This sample was found to have the highest degree of densification connected to highest strength (even higher than for reference sample).

4.2.1 Hardness and fracture toughness

Even though the carbon nanotubes containing nanocomposites were proposed with the aim of improving mechanical performance, there is a trade-off between various properties. Typically, the introduction of carbon phases into a ceramics leads to lower hardness and its effect on the fracture toughness is ambiguous, even though there are some toughening mechanisms present in the crack, such as crack deflection, crack bridging and fibers pull-out.

Early examples represent hot pressed (2273 K) CNTs–SiC composites, investigated by Ma et al., 1998, which showed an increase of 10% in the strength and fracture toughness compared to SiC ceramics prepared with the same method. Alumina–CNT composites were also investigated in some depths by several authors. In contrast to reports of Peigney et al., 2000, and Flahaut et al., 2000, which did not observe an improvement of the mechanical properties of CNT–metal–alumina composites obtained by hot-pressing, Siegel et al., 2001, measured an increase in fracture toughness of 24% (from 3.4 up to 4.2 $MPa.m^{1/2}$) in MWCNT–alumina composites (10% in vol) prepared by hot-pressing. Zhan et al., 2003a, reported of dense alumina–SWNT composites possessing a toughness of 9.7 $MPa.m^{1/2}$, i.e. three times higher than that of pure alumina (3.3 $MPa.m^{1/2}$).

The reason given for the high performances of the as-prepared materials are the optimum dispersion of the CNTs and the process of spark plasma sintering performed at lower temperatures (1100 °C) with consequent lower damaging of the CNTs compared to traditional hot-pressing, (Borrell et al., 2010; Lupo et al., 2004).

Sun (Sun et al., 2005) studied the mechanical and fracture behavior of MWCNT/3Y-TZP composites containing 0.1–1.0 wt.% MWCNTs and SWCNTs prepared by SPS. They found that the addition of CNTs had a negative influence on the hardness of the composites and no influence (at 0.5 wt.%) or a negative influence on the fracture toughness. Comparing the influence of the addition of SWCNTs and MWCNTs on the fracture toughness, they found that the MWCNT are slightly more effective in the toughening. However, they used the

indentation technique for the toughness measurements, which is useful only for comparison purposes, cannot be considered a true material characterization. Similar results were found in (Ukai et al., 2006), where the failure properties of similar materials were studied. According to these works, the CNTs often agglomerate at the ZrO_2 boundaries, and the weak bonding between the CNTs and zirconia are the reason why the reinforcing effect of the CNTs is limited. The results of (Duszová et al., 2008a) found for zirconia with carbon nanofibers are in a very good agreement with these results (Fig. 10) and show that even the use of relatively coarse whisker-like CNFs is not effective in toughening the zirconia ceramic matrix at the current amounts used. On the other hand, it was noted that on the fracture surface/line different toughening mechanisms were found, mainly in the form of crack deflection at the CNFs. The reason for the relatively low indentation fracture toughness is probably the poor dispersion and therefore the limited toughening effect of the CNFs.
The indentation toughness of monolithic alumina is approximately 3.24 MPa.m$^{1/2}$, which is comparable to similar materials in the literature. The addition of 2 % carbon black increased the indentation toughness, but after increasing to 5 % the indentation toughness decreased to the similar level as of the monolithic material. The addition of 5 % CNTs increased the indentation toughness up to 4.14 MPa.m$^{1/2}$ which is the highest value obtained for the materials investigated.

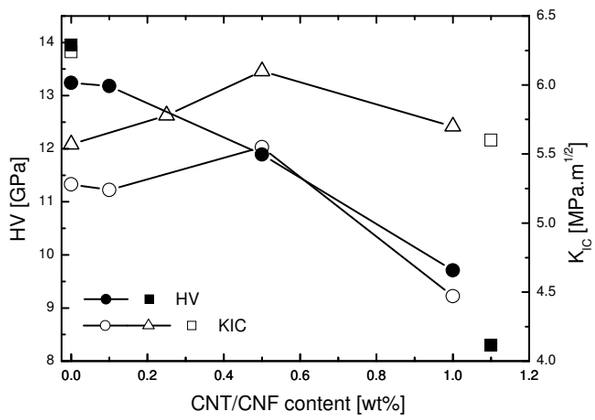

Fig. 10. Influence of the CNT/CNF addition on the Vickers hardness and indentation toughness of zirconia based composites. After Sun et al 2005 (circles), Ukai et al. 2006 (triangles), and Duszová et al 2008 (squares).

Fractography of the fracture surfaces of the composites revealed carbon based "bridges" between the alumina grains, which probably in the case of Al_2O_3 - CNT composite are strong enough to increase the resistance against the crack propagation. These results are in good agreement with the results of recent investigations of Ahmad (Ahmad et al., 2010). There, well-dispersed CNT-reinforced Al_2O_3 nanocomposites were prepared with reasonably high density using hot pressing. It was shown that 2 wt. % of CNT addition increased the hardness, flexural strength and fracture toughness of nanocomposites (from 3 to 4.3 MPa.m$^{1/2}$). Further CNT addition up to 5 wt. % slightly decreased the hardness, reduced the flexural strength but improved the toughness up to 4.5 MPa.m$^{1/2}$. The increase in toughness is believed to be associated with the strong interface connections between the CNT and the matrix, resulting in pullout resistance, bridged the crack gaps and hindered the crack propagation by exploiting CNTs elasticity, leading to improved fracture toughness.

4.2.2 Tribological properties

Fig. 11 shows examples of development of the friction coefficient over the test running distance (Hvizdoš et al., 2011a). In all cases was friction after short initial stage (in order of meters) rather stable and reproducible. For monolithic ZrO_2 the values of COF were slightly lower than similar results found in literature. The sliding wear behaviour of ZrO_2 using the ball on disk method and alumina as a friction partner was also investigated in (Suh et al., 2008). The applied loads ranged from 19.8 N to 98 N. There, the coefficient of friction varied between 0.6 and 0.7 depending on the sliding speed, and appeared to be independent on the applied load. Higher COF can be explained by the damage mechanisms - the alumina grains detached from the alumina surface and caused abrasion of zirconia. For lower applied load, however, the main wear mechanism in the zirconia is typically self-polishing by low intensity abrasion.

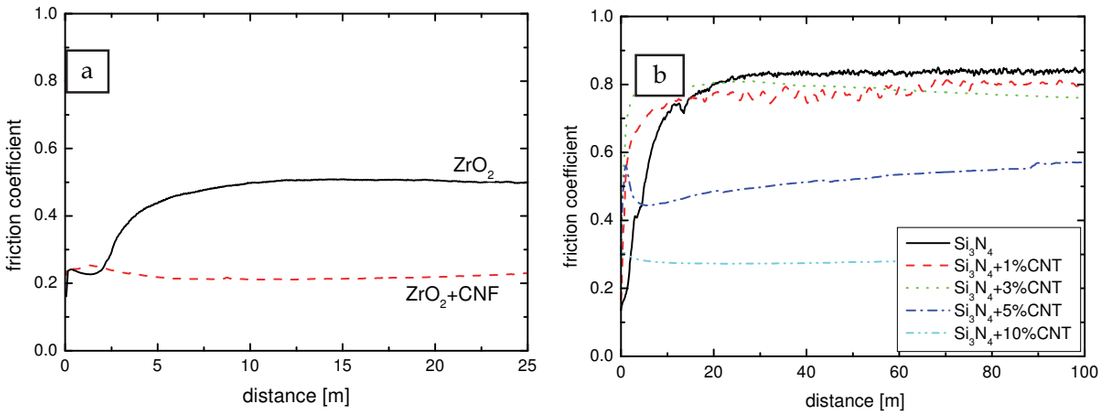

Fig. 11. Friction coefficient during the testing under similar conditions. (a) ZrO_2 based materials tested at 1 N load; (b) Si_3N_4 based materials at 1.5 N load, (Hvizdoš et al., 2011a).

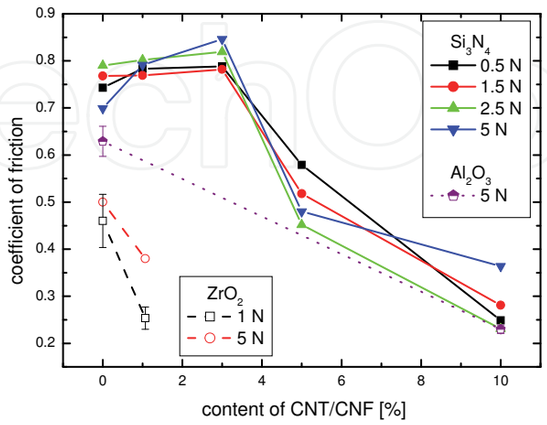

Fig. 12. Coefficient of friction as function of amount of carbon phases in the CMC materials (Hvizdoš et al., 2011a; Hvizdoš et al., 2011b).

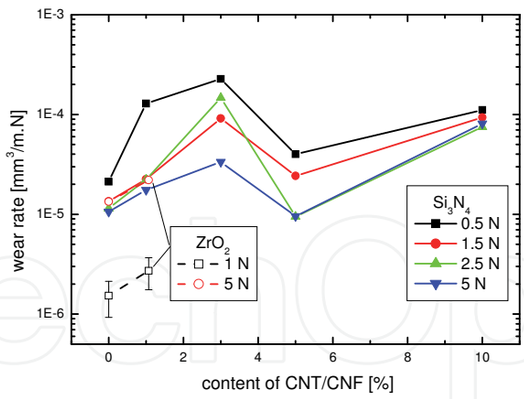

Fig. 13. Dependence of wear resistance of the experimental materials on their carbon content tested at various load levels.

Self-mated wear of monolithic silicon nitride was studied in various situations and can be summarized both in terms of the friction coefficient (Fig. 11b and 12, values 0.7-0.8) and wear rates (Fig. 13, values 1-2x10^{-5}mm^3/N.m) (Kašiarová et al., 2004; Hvizdoš et al., 2011a).
Fig. 12 summarizes the average values of friction for all materials. The Si_3N_4 based materials exhibited higher friction due to chemical similarity of both friction partners, particularly for low CNT contents. Here, the COF started to decrease only when the CNT content reached ~5 wt%. In Si_3N_4-10%CNT the COF values dropped to ~0.2 which was comparable to the values for ZrO_2-CNF. Similar values were found for self mated friction of alumina (Hvizdoš et al., 2011b). Here, only monolith and 10% CNT containing composite are given, but the tendency is very similar to that of silicon nitride materials and more than 60% reduction of friction coefficient was reported.
Fig. 13 shows the wear rates of various materials at different loads. Generally, the presence of CNT/CNF tends to decrease the wear resistance due to less than optimal microstructure. However, Hvizdoš et al., 2011a, found a sort of an optimum for fractions of around 5% CNT, where the wear resistance improved, probably thanks to significantly reduced friction. Then for Si_3N_4-10%CNT it only reached values similar to those for Si_3N_4-1%CNT.
Fig. 14 illustrates typical damage observed in the wear tracks. The wear testing of the monolithic materials of both types of materials left faint, quite smooth wear tracks with polished look, as it is shown in Fig 14a and 14c for sliding at 5N load. This is consistent with the low wear rates of materials with high quality microstructure.
Figs 14b and 14d illustrate the wear tracks of the composite materials and present the micromechanisms of the wear surface damage. Microscopic observations of the worn surface of the ZrO_2-CNF composite showed pulled out CNFs (Fig. 14b) and suggested the presence of a smeared layer of graphite and crushed CNFs, the so-called transferred film, which significantly lowers the friction coefficient, even though relatively low amount of carbon (1.07wt%) was incorporated into the microstructure. As Fig. 14d as well as the values of COF and wear rates suggest, the CNTs in silicon nitride based composites were much less effective in creating the transferred film. It may be due to their greater mechanical stability and better distribution throughout the microstructure. This could mean that their pull-out and also their destruction in the contact zone are more difficult.
In all cases by incorporating appropriate amount of carbon filaments the coefficient of friction between 0.2 and 0.3 was achieved. A similar lubricating effect by carbon phases was

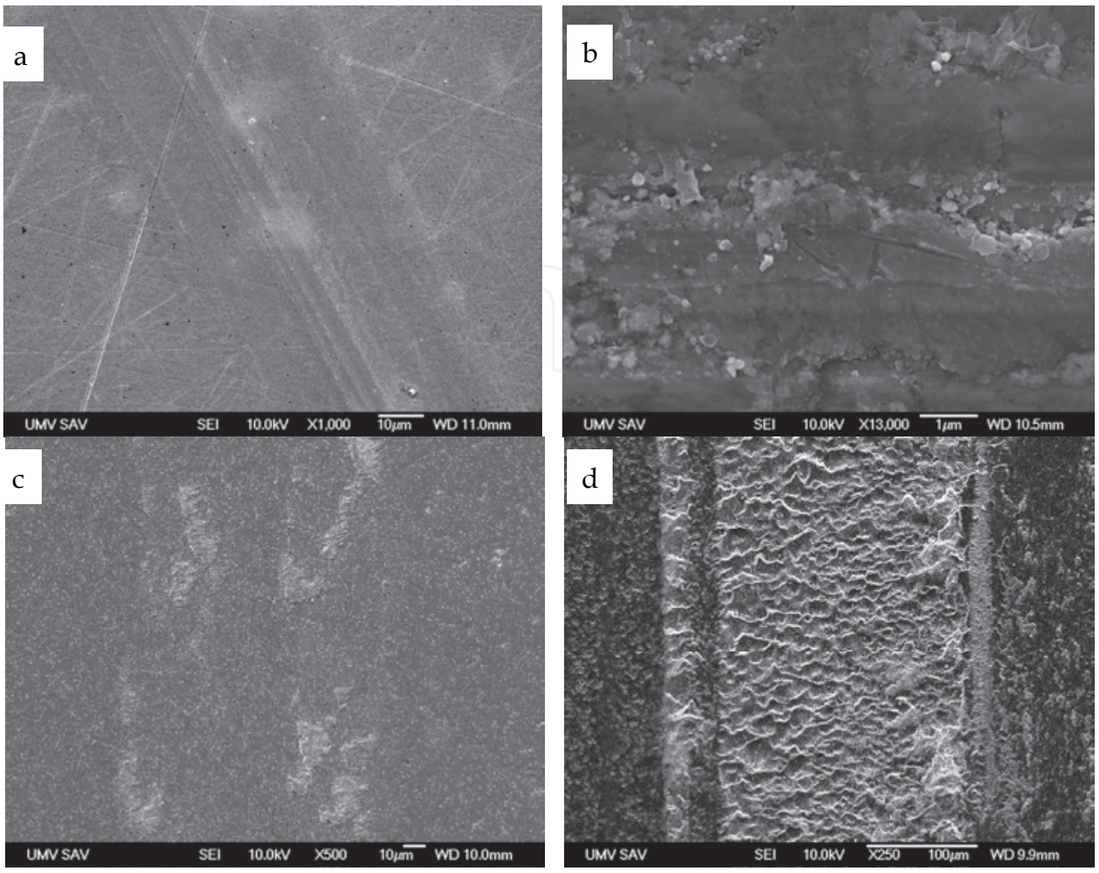

Fig. 14. Wear damage at normal load 5N: (a) smooth wear tracks in monolithic ZrO_2; (b) detail of the wear track in ZrO_2-CNF composite – pull-out of CNFs and smeared transferred film; (c) monolithic Si_3N_4 - smooth track with polished look; (d) Si_3N_4-3%CNT – surface abrasion.

reported for MWCNTs-containing Al_2O_3 composites by (An et al., 2003) and (Yamamoto et al., 2008a) and for SWCNT solids by (Yamamoto et al., 2008b). In (An et al., 2003) the authors reported a 40% decrease in friction coefficient in 12 wt.% MWCNT–Al_2O_3 composite down to the value of 0.3. Yamamoto with co-workers, for their composites reached the minimum of the friction coefficient (with the value of 0.3) at 4 mass% of MWCNT content. According to An et al. the rolling motion of CNTs at the interface between the specimen and the ball can probably lower the friction coefficient as well. This effect in the case of ZrO_2-CNF composite was not proven. Our results for silicon nitride based composites are in a very good agreement with the results reported for SWCNT solids sliding against Si_3N_4 where steady-state friction coefficients of 0.22-0.24 were found.

Alumina–CNT composites with CNT contents from 0 to 12 wt. % were fabricated by two different processing techniques by Lim et al. (Lim et al., 2005) in order to compare the effect of fabrication techniques on the tribological properties of CNT added alumina composites. Superior tribological properties were achieved by introduction of tape casting, followed by lamination and hot pressing. Wear loss decreased significantly and friction coefficients were maintained to be about the same by addition of the CNTs up to 12 wt. %. Agglomeration of CNTs, frequently observed with hot-pressed specimens, was significantly reduced and

relatively uniform distribution of CNTs was obtained. The effective dispersion of CNTs contributed to the densification of composites and to superior mechanical and tribological properties of CNT added alumina composites.

4.3 Electrical properties

The conductivity of an individual CNT can be metallic or semiconducting, depending on the chirality of the CNT with axial component extremely high, 2×10^7 S/m (Ebbesen et al., 1996) comparable to that of silver, cooper or gold. Larger CNFs have properties similar to graphite. As it was shown in the section on microstructure, the CNTs and CNFs can be distributed along matrix grain boundaries and/or between matrix grains. When interconnected they can form continuous networks. Such networks in CNT/CNF nanocomposites can be electrically conductive thanks to various mechanisms that involve fluctuation-assisted tunnelling or variable range hopping between the individual nanofibers.

Inam et al., 2010, collected and summarized a number of studies of electrical properties of various CMCs prepared by hot-pressing and SPS. It seems that about 5 to 10 wt.% of carbon filament phases is necessary to ensure the percolation of electrical charges, and conductivities in orders of tens or hundreds S/m were found. Generally speaking, the carbon black, which was used for reference reasons, is less efficient, while larger CNFs or higher amounts of SWNT+MWNT form more conductive networks (588 S/m for HP alumina-5%CNF, and 853 S/m for magnesium aluminate-12.2%CNT, respectively).

Similar results were found recently for series of zirconia, alumina and silicon nitride based CMCs (Duszová et al., 2008b; Hvizdoš et al., 2011b). These results are summarized in Fig. 15. Here, for the materials with CNTs, the percolation threshold was between 3 and 5 wt.% for Si_3N_4 and between 2 and 5 wt% for alumina. For the latter composite the electrical conductivity increased from practically zero to the maximum value of 140 S/m for 10 wt.% of CNTs. Analogous materials prepared in the same way but with admixture of carbon black yielded electrical conductivity about an order of magnitude lower – e.g. for 5 wt% of additive it was 90.5±4.8 S/m for CNTs and 8.5±0.1 S/m for carbon black. This means that the size and shape of the mixed carbon black additives resulted in a limited graphite particle connection in the matrix, which was much less efficient in securing the percolation as it is illustrated schematically in Fig. 16.

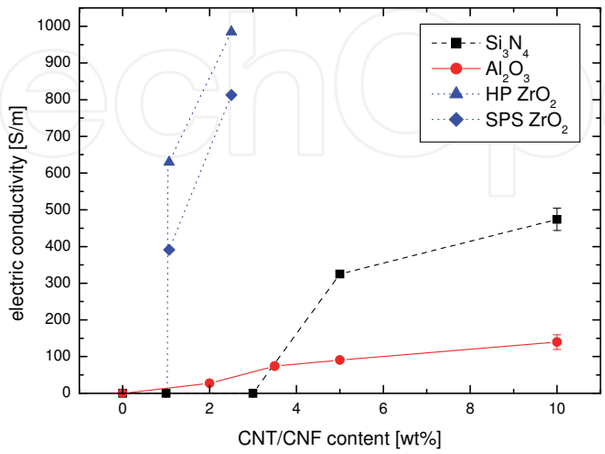

Fig. 15. Electrical conductivity – illustration of percolation theshold for different CMC-CNT /CNF composites (Duszová et al., 2008b; Hvizdoš et al., 2011b).

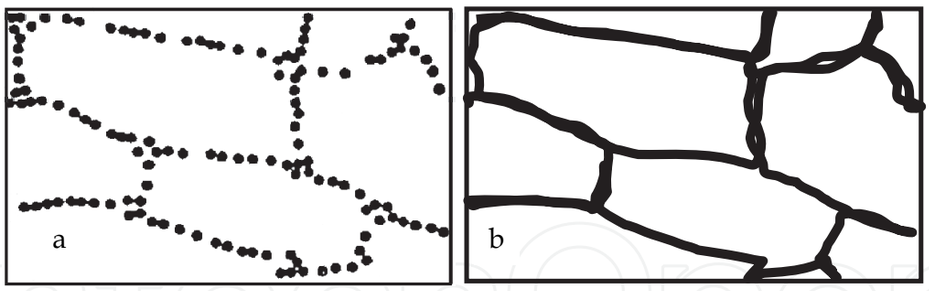

Fig. 16. Scheme of the microstructure of CMC with carbon black (a) and CNTs (b).

Carbon nanofibers were significantly more efficient, as shown in the case of ZrO_2-CNF composites (Fig. 15), where amounts as low as 1 to 3 wt.% of carbon nanofibers were sufficient to increase the electrical conductivity from ~10^{-12} S/m to 983± 200 S/m (hot pressed) or 813±273 S/m (SPSed), (Duszová et al., 2008b).
In summary it can be concluded that thanks to their fibrous nature and intergranular distribution, very little amount of carbon nanofibers (only about 1-5 wt%, depending on the basic material microstructure) is sufficient for the percolation effect to take place. In this way an increase in electrical conductivity by more than 13 orders of magnitude can be achieved.

5. Conclusion

The processing routes, microstructure characteristics, mechanical and functional properties of carbon nanofibers containing CMCs have been a subject of intensive study during last 10-15 years. The result show that introduction of CNTs/CNFs usually results in finer microstuctures. It also invariably leads to a drop in hardness. As for the fracture toughness, up to now the results are ambiguous. In most cases the fracture toughness decreases, particularly for higher fractions of carbon phases. Yet, the potential for improving in this area by toughening mechanisms such as fiber pull-out, crack bridging and deflection has been recognized. In this respect future work is necessary to optimize the interface between the matrix and the fibers, which will ensure good bonding of the two phases, yet allowing the toughening mechanisms to be active.
The tribological studies showed clear benefits of presence of carbon fibers. By a small amount of CNFs (as little as 1 wt%) the coefficient of friction of ZrO_2 can be lowered from 0.45 to 0.2 by formation of carbon film which acts as a solid lubricant. The CNTs are slightly less effective and higher amount is necessary to achieve similar results. The wear resistance generally decreases, which can be correlated to lower hardness and fracture toughness, but in several instances a sort of optimum was found (e.g. Si_3N_4-5wt%CNT) where the wear rate was similar to that of monolithic material but with much lower coefficient of friction.
The electrical conductivity can be increased very significantly and low amounts of CNFs or CNTs are sufficient to change an insulator to a functionalized conductive ceramics. Here again larger CNFs seem to be more effective and show clear potential for future development of carbon nanofibers containing ceramic matrix materials.

6. Acknowledgement

This work was done within the frame of the project „Centre of Excellence of Advanced Materials with Nano- and Submicron- Structure“, which is supported by the Operational

Program "Research and Development" financed through European Regional Development Fund. The experiments were supported by the projects VEGA 2/0120/10 and COST Action MP0701. The authors would like to express their gratitude to C. Balázsi, J. Kuebler, G. Blugan, M. Reece, and others for the preparation of the experimental materials and to J. Morgiel and his co-workers for the TEM studies.

7. References

Ahmad, I.; Unwin, M.; Cao, H.; Chen, H.; Zhao, H.; Kennedy, A. & Zhu, Y.Q. (2010). Multi-walled carbon nanotubes reinforced Al_2O_3 nanocomposites: Mechanical properties and interfacial investigations, *Composites Science and Technology*, Vol. 70, No.4 (August 2010), pp. 1199–1206, ISSN 0266-3538

Al-Saleh, M.H. & Sundararaj, U. (2009). A review of vapor grown carbon nanofiber/polymer conductive composites, *Carbon*, Vol. 47, No.1 (January 2009), pp. 2–22, ISSN 0008-6223

An, J.W.; You, D.H. & Lim, D.S. (2003). Tribological properties of hot-pressed alumina-CNT composites, *Wear*, Vol. 255, No.1 (August 2003), pp.677-681, ISSN: 0043-1648

Anstis, G.R.; Chantikul, P.; Lawn, B. & Marshall, D. (1981). A critical evaluation of indentation techniques for measuring fracture toughness: I. Direct crack measurements, *Journal of the American Ceramic Society*, Vol. 64, No.9 (September 1981), pp. 533-538, ISSN 0002-7820

Balázsi, C.; Kónya, Z.; Wéber, F.; Biró, L.P. & Arató, P. (2003). Preparation and characterization of carbon nanotube reinforced silicon nitride composites. *Material Science and Engineering C*, Vol. 23, No. 6-8 (December 2003), pp. 1133–1137, ISSN 0928-4931

Balázsi, C.; Kónya, Z.; Kasztovszky, Z.; Wéber, F.; Vértesy, Z. & Biró, L.P. (2004). Examination of the carbon nanotube reinforced silicon nitride composites. In *Proc. of the 5th international conference on high temperature ceramic matrix composites (HTCMC-5),* New Frontiers and Horizons, Seattle, Washington, DC: American Ceramic Society; September 2004. pp. 107–112.

Balázsi, C.; Fényi, B.; Hegman, N.; Kovér, Z.; Wéber, F.; Vértesy, Z.; Kónya, Z.; Kiricsi, I.; Biró, L.P. & Arató, P. (2006). Development of CNT/ Si_3N_4 composites with improved mechanical and electrical properties, *Composites: Part B*, Vol. 37, No.6, pp. 418–424, ISSN 1359-8368

Belmonte, M.; González-Julián, J.; Miranzo, P. & Osendi, M.I. (2010). Spark plasma sintering: A powerful tool to develop new silicon nitride-based materials, *Journal of the European Ceramic Society*, Vol. 30, No. 14 (October 2010), pp. 2937–2946, ISSN 0955-2219

Borrell, A.; Fernandez, A.; Merino, C. & Torrecillas, R. (2010). High density carbon materials obtained at relatively low temperature by spark plasma sintering of carbon nanofibers. *International Journal of Materials Research*, Vol.101, No.1, pp. 112-116, ISSN 1862-5282

Callister, W.D. (2003). *Materials Science and Engineering: An Introduction*, 6th ed. Wiley, New York. ISBN 978-0471736967

Cha, S.I.; Kim, K.T.; Lee, K.H.; Mo, C.B. & Hong, S.H. (2005). Strengthening and toughening of carbon nanotube reinforced alumina nanocomposite fabricated by molecular

level mixing process, *Scripta Materialia*, Vol. 53, No. 7 (October 2005), pp.793-797, ISSN 1359-6462

Datye, A.; Wu, K.-H.; Gomes, G.; Monroy, V.; Lin, H.-T.; Vleugels, J. & Vanmeensel, K. (2010). Synthesis, microstructure and mechanical properties of 3YTZP-MWNTs nanocomposite by direct in-situ growth of MWNTs on Zirconia particles. *Composite Science and Technology*, Vol.70, No.14, pp. 2086-2092, ISSN 0266-3538

Dusza, J. & Šajgalík, P. (2009). *Silicon nitride and alumina-based nanocomposites, Handbook of nanoceramics and their based nanodevices 2*, Stevenson Ranch, American Scientific Publishers, pp. 253-283, ISBN 1-58883-116-7

Dusza, J.; Blugan, G.; Morgiel, J.; Kuebler, J.; Inam, F.; Peijs, T.; Reece, M.J. & Puchý, V. (2009). Hot pressed and spark plasma sintered zirconia/carbon nanofiber composites, *Journal of the European Ceramic Society*, Vol. 29, No. 15 (December 2009), pp. 3177–3184, ISSN 0955-2219

Duszová, A.; Dusza, J.; Tomášek, K.; Morgiel, J.; Blugan, G. & Kuebler, J. (2008a). Zirconia/carbon nanofiber composite, *Scripta Materialia*, Vol. 58, No. 6 (March 2008), pp. 520-523, ISSN 1359-6462

Duszová, A.; Dusza, J.; Tomášek, K.; Blugan, G. & Kuebler, J. (2008b). Microstructure and properties of carbon nanotube/zirconia composite, *Journal of the European Ceramic Society*, Vol. 28, No. 5, pp. 1023-1027, ISSN 0955-2219

Ebbesen, T. W., Lezec, H. J., Hiura, H., Bennett, J. W., Ghaemi, H. F. & Thio, T., (1996). Electrical-conductivity of individual carbon nanotubes. *Nature*, Vol. 382, (July 1996), pp. 54–56, ISSN: 0028-0836

Endo, M.; Kim, Y.A.; Hayashi, T.; Fukai, Y.; Oshida, K.; Terrones, M.; Yanagisawa, T.; Higaki, S. & Dresselhaus, M.S. (2002). Structural characterization of cup-stacked-type nanofibers with an entirely hollow core, *Applied Physics Letters*, Vol. 80, No. 7 (February 2002), pp. 1267-1268, ISSN 0003-6951

Flahaut, E.; Peigney, A.; Laurent, Ch.; Marliére, C.; Chastel, F. & Rousset, A. (2000). Carbon nanotube-metal-oxide: microstructure, electrical conductivity mechanical properties, *Acta Materialia*, Vol. 48, No. 14 (September 2000), pp. 3803–3812, ISSN 1359-6454

Garmendia, N.; Santacruz, I.; Moreno, R. & Obieta, I. (2010). Zirconia-MWCNT nanocomposites for biomedical applications obtained by colloidal processing. *Journal of Materials Science-Materials in Medicine*, Vol.21, No.5, pp. 1445-1451, ISSN: 0957-4530

Garvie, R.C.; Hannink, R.H. & Pascoe, R.T. (1975). Ceramic steel?, *Nature*, Vol. 258, (December 1975), pp. 703–704, ISSN 0028-0836

Garvie, R.C.; Urbani, C.; Kennedy, D.R. & McNeuer, J.C. (1984). Biocompatibility of magnesia-partially stabilized zirconia (Mg-PSZ) ceramics, *Journal of Materials Science*, Vol. 19, No. 10, pp. 3224-3228, ISSN: 0022-2461

González-Julián, J.; Schneider, J.; Miranzo, P.; Osendi, M.I. & Belmonte, M. (2010). Tribologische Charakterisierung von Si_3N_4-CNT-Kompositkeramiken unter ungeschmierter und mediengeschmierter oszillierender Gleitbeanspruchung, in *Proc. „Tribologie-Fachtagung 2010“*, Deutsche Gesellschaft für Tribologie (GFT), Aachen, pp. 02/1 - 02/10

Hvizdoš, P.; Puchý, V.; Duszová, A. & Dusza J. (2010). Tribological behavior of carbon nanofiber–zirconia composite, *Scripta Materialia*, Vol. 63, No. 2 (July 2010), pp. 254–257, ISSN 1359-6462

Hvizdoš, P.; Duszová, A.; Puchý, V.; Tapasztó, O.; Kun, P.; Dusza, J. & Balázsi, C. (2011a). Wear behavior of ZrO_2-CNF and Si_3N_4-CNT nanocomposites, *Key Engineering Materials*, Vol. 465, pp. 495-498, ISBN-13 978-3-03785-006-0

Hvizdoš, P; Puchý, V; Duszová, A.; Dusza, J. (2011b). Tribological and electrical properties of ceramic matrix composites with carbon nanotubes, in *Engineering Ceramics 2011*, Smolenice, Slovakia, (May 8-12, 2011), in press

Iijima, S. (1991). Helical microtubules of graphitic carbon, *Nature*, Vol. 354, (November 1991), pp. 56-58, ISSN 0028-0836

Inam, F.; Yan, H.; Jayaseelan, D.D.; Peijs, T. & Reece, M.J. (2010). Electrically conductive alumina–carbon nanocomposites prepared by Spark Plasma Sintering, *Journal of the European Ceramic Society,* Vol. 30, pp. 153–157, ISSN: 0028-0836

ISO 20808:2004(E), "Fine ceramics – Determination of friction and wear characteristics of monolithic ceramics by ball-on-disc method", (2004).

Kašiarová, M.; Rudnayová, E.; Dusza, J.; Hnatko, M.; Šajgalík, P.; Merstallinger, A. & Kuzsella, L. (2004). Some tribological properties of a carbon-derived Si3N4/SiC Nanocomposite, *Journal of the European Ceramic Society*, Vol. 24, No.12, pp. 3431–3435, ISSN 0955-221

Krishnan, A.; Dujardin, E.; Treacy, M.M.J.; Hugdahl, J.; Lynum, S. & Ebbesen, T.W. (1997). Graphitic Cones and the Nucleation of Curved carbon Surfaces, *Nature*, Vol. 388, (July 1997), pp. 451–454, ISSN 0028-0836

Lee, S.; Kim, T.R.; Ogale, A.A. & Kim M.S. (2007). Surface and structure modification of carbon nanofibers. *Synthetic Metals*, Vol. 157, No. 16-17 (August 2007), pp. 644-650, ISSN 0379-6779

Lee, C.J.; Lyu, S.C; Kim, H.W.; Lee, J.H. & Cho, K.I. (2002). Synthesis of bamboo-shaped carbon–nitrogen nanotubes using C_2H_2–NH_3–$Fe(CO)_5$ system, *Chemical Physics Letters*, Vol. 359, No. 1-2 (June 2002), pp. 115-120, ISSN 0009-2614

Lim, D.S.; You, D.H.; Choi, H.J.; Lim, S.H. & Jang, H. (2005). Effect of CNT distribution on tribological behavior of aluminum-CNT composites. *Wear*, Vol. 259, No. 1-6 (July-August 2005), pp. 539-544, ISSN 0043-1648

Longtin, R.; Fauteux, C.; Goduguchinta, R. & Pegna, J. (2007). Synthesis of carbon nanofiber films and nanofiber composite coatings by laser-assisted catalytic chemical vapor deposition, *Thin Solid Films*, Vol. 515, No. 5 (January 2007), pp. 2958-2964, ISSN 0040-6090

Lupo, F.; Kamalakaran, R.; Scheu, C.; Grobert, N. & Ruhle, M. (2004). Microstructural investigations on zirconium oxide-carbon nanotube composites synthesized by hydrothermal crystallization, *Carbon*, vol. 42, no. 10, pp. 1995-1999, ISSN 0008-6223

Ma, R.Z.; Wu, J.; Wei, B.Q.; Liang, J. & Wu, D.H. (1998). Processing and properties of carbon nanotubes-nano-SiC ceramic. *Journal of Material Science*, Vol. 33, No. 21 (November 1998), pp. 5243–5463, ISSN 0022-2461

Mazaheri, M.; Mari, D.; Hesabi, Z.R.; Schaller, R. & Fantozzi, G. (2011). Multi-walled carbon nanotube/nanostructured zirconia composites: Outstanding mechanical properties in a wide range of temperature. Composites Science and Technology, in press, doi:10.1016/j.compscitech.2011.01.017

McEnaney, B. (2001). Carbon and graphites, mechanical properties of, *Encyclopedia of Materials: Science and Technology*, Amsterdam, New York, pp. 967–975, ISBN 978-0080431529

Melechko, A.V.; Merkulov, V.I.; McKnight, T.E.; Guillorn, M.A.; Klein, K.L.; Lowndes, D.H. & Simpson, M.L. (2005). Vertically aligned carbon nanofibers and related structures: Controlled synthesis and directed assembly, *Journal of Applied Physics*, Vol. 97, No.4 (February 2005), 041301, ISSN 0021-8979

Morrell, R. (1985). *Handbook of properties of technical and engineering ceramics*, Part 1., HMSO, London, ISBN 978-0114800529

Mukhopadhyay, A.; Chu, B.T.T.; Green, M.L.H. & Todd, R.I. (2010). Understanding the mechanical reinforcement of uniformly dispersed multiwalled carbon nanotubes in alumino-borosilicate glass ceramic. *Acta Materialia*, Vol.58, No.7 (April 2010), pp. 2685-2697, ISSN 1359-6454

Peigney, A.; Laurent, Ch.; Flahaut, E. & Rousset, A. (2000). Carbon nanotubes in novel ceramic matrix nanocomposites, *Ceramics International*, Vol. 26, No. 6 (July 2000), pp. 677–683, ISSN 0272-8842

Perera, D.S.; Tokita, M. & Moricca, S. (1998). Comparative study of fabrication of Si_3N_4/SiC composites by spark plasma sintering, *Journal of European Ceramic Society*, Vol. 18, No.4 (April 1998), pp. 401-404, ISSN: 0955-2219

Puchý, V.; Tatarko, P.; Dusza, J.; Morgiel, J.; Bastl, Z. & Mihaly, J. (2010). Characterization of carbon nanofibers by SEM, TEM, ESCA and Raman spectroscopy, *Kovove Materialy-Metallic Materials*, Vol. 48, No. 6, pp. 379-385, ISSN: 0023-432X

Ruoff, R.S.; Qian, D. & Liu, W.K. (2003). Mechanical properties of carbon nanotubes: theoretical predictions and experimental measurements. *Comptes Rendus Physique*. Vol. 4, No.9 (November 2003), pp. 993-1008, ISSN 1631-0705

Siegel, R.W.; Chang, S.K.; Ash, B.J.; Stone, J.; Ajayan, P.M.; Doremus R.W. & Schadler R.S. (2001). Mechanical behaviour of polymers and ceramics matrix nanocomposites, *Scripta Materialia*, Vol. 44, No.8 (May 2001), pp. 2061–2064, ISSN 1359-6462

Shi, S.L. & Liang, J. (2006). Effect of Multiwall Carbon Nanotubes on Electrical and Dielectric Properties of Yttria-Stabilized Zirconia Ceramic. *Journal of the American Ceramic Society*, Vol. 89, No. 11 (November 2006), pp. 3533–3535, ISSN 0002-7863

Shi, S.L. & Liang, J. (2007). Electronic transport properties of multiwall carbon nanotubes / yttria-stabilized zirconia composites, *Journal of Applied Physics*, Vol. 101, No.2, p. 023708, ISSN 0021-8979

Suh, M.S.; Chae, Y.H. & Kim, S.S. (2008). Friction and wear behavior of structural ceramics sliding against zirconia, *Wear*, Vol. 264, No. 9-10, (April 2008), pp. 800–806, ISSN 0043-1648

Sun, J.; Gao L.; Iwasa, M.; Nakayama, T. & Niihara, K. (2005). Failure investigation of carbon nanotube/3Y-TZP nanocomposites, *Ceramics International*, Vol 31, No. 8, pp. 1131-1134, ISSN 0272-8842

Tatami, J.; Katashima, T.; Komeya, K.; Meguro, T. & Wakihara, T. (2005). Electrically Conductive CNT-Dispersed Silicon Nitride Ceramics. *Journal of the American Ceramic Society*, Vol. 88, No. 10 (October 2005), pp. 2889–2893, ISSN 0002-7863

Ukai, T.; Sekino, T.; Hirvonen, A.; Tanaka, N.; Kusunose, T.; Nakayama, T. & Niihara, K. (2006) Preparation and electrical properties of carbon nanotubes dispersed zirconia nanocomposites, *Key Engineering Materials*, Vol.317-318, pp.661-664, ISSN 1662-9795

Yamamoto, G.; Omori, M.; Yokomizo, K.; Hashida, T. & Adachi, K. (2008a). Structural Characterization and Frictional Properties of Carbon Nanotube/Alumina Composites Prepared by Precursor Method, *Material Science and Engineering B*, Vol. 148, No. 1-3 (February 2008) pp. 265-269, ISSN 0921-5107

Yamamoto, G.; Hashida, T.; Adachi, K. & Takagi, T. (2008b). Tribological Properties of Single-Walled Carbon Nanotube Solids, *Journal of Nanoscience and Nanotechnology*, Vol. 8, No. 5 (May 2008), pp. 2665-2670, ISSN 1550-7033

Yu, M.F.; Lourie, O.; Dyer, M.J.; Moloni, K.; Kelly, T.F. & Ruoff, R.S. (2000). Strength and breaking mechanism of multiwalled carbon nanotubes under tensile load, *Science*, Vol. 287, No. 5453 (January 2000), pp. 637-640, ISSN 0036-8075

Zhan, G.-D.; Kuntz, J.D.; Wan, J & Mukherjee, A.K. (2003a). Single-wall carbon nanotubes as attractive toughening agents in alumina-based nanocomposites. *Nature Materials,* Vol.2, No. 1 (January 2003), pp. 38–42, ISSN 1476-1122

Zhan, G.-D.; Kuntz, J.D.; Garay, J.E. & Mukherjee, A.K. (2003b). Electrical properties of nanoceramics reinforced with ropes of single-walled carbon nanotubes. *Applied Physics Letters,* Vol. 83, No. 6 (August 2003), pp. 1228-1230, ISSN 0003-6951

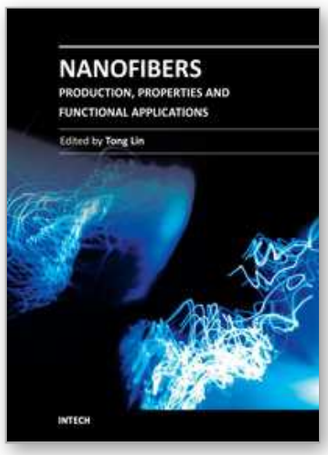

Nanofibers - Production, Properties and Functional Applications
Edited by Dr. Tong Lin

ISBN 978-953-307-420-7
Hard cover, 458 pages
Publisher InTech
Published online 14, November, 2011
Published in print edition November, 2011

As an important one-dimensional nanomaterial, nanofibers have extremely high specific surface area because of their small diameters, and nanofiber membranes are highly porous with excellent pore interconnectivity. These unique characteristics plus the functionalities from the materials themselves impart nanofibers with a number of novel properties for advanced applications. This book is a compilation of contributions made by experts who specialize in nanofibers. It provides an up-to-date coverage of in nanofiber preparation, properties and functional applications. I am deeply appreciative of all the authors and have no doubt that their contribution will be a useful resource for anyone associated with the discipline of nanofibers.

How to reference
In order to correctly reference this scholarly work, feel free to copy and paste the following:

Pavol Hvizdoš, Viktor Puchý, Annamária Duszová and Ján Dusza (2011). Carbon Nanofibers Reinforced Ceramic Matrix Composites, Nanofibers - Production, Properties and Functional Applications, Dr. Tong Lin (Ed.), ISBN: 978-953-307-420-7, InTech, Available from: http://www.intechopen.com/books/nanofibers-production-properties-and-functional-applications/carbon-nanofibers-reinforced-ceramic-matrix-composites

INTECH
open science | open minds

InTech Europe
University Campus STeP Ri
Slavka Krautzeka 83/A
51000 Rijeka, Croatia
Phone: +385 (51) 770 447
Fax: +385 (51) 686 166
www.intechopen.com

InTech China
Unit 405, Office Block, Hotel Equatorial Shanghai
No.65, Yan An Road (West), Shanghai, 200040, China
中国上海市延安西路65号上海国际贵都大饭店办公楼405单元
Phone: +86-21-62489820
Fax: +86-21-62489821

IntechOpen